Applied Catalysis B: Environmental 191 (2016) 138–146

Contents lists available at ScienceDirect

Applied Catalysis B: Environmental

journal homepage: www.elsevier.com/locate/apcatb

Iridium addition enhances hydrodesulfurization selectivity in 4,6-dimethyldibenzothiophene conversion on palladium

Hessam Ziaei-Azad, Natalia Semagina*

Department of Chemical and Materials Engineering, University of Alberta, 9211-116 St., Edmonton, AB T6G 1H9, Canada

ARTICLE INFO

Article history:
Received 17 January 2016
Received in revised form 6 March 2016
Accepted 11 March 2016
Available online 14 March 2016

Keywords:
Bimetallic nanoparticles
HDS
PVP
Benzothiophene
Hydrotreating

ABSTRACT

38% to 93% selectivity enhancement toward sulfur-free products was observed upon iridium addition to a palladium-only catalyst in the hydrodesulfurization of a refractory sulfur compound 4,6-dimethyldibenzothiophene (4,6-DMDBT) at the same 40% conversion from a 300 ppm, S-containing feed at 5 MPa and 300 °C. Pd promoted hydrogenation to sulfurous intermediates, while Ir catalyzed C—S hydrogenolysis and also improved Pd resistance to sintering. The selectivity in the direct desulfurization path for the Ir-containing catalysts increased up to 26% versus 5% for the Pd-only catalyst. The bimetallic catalyst allowed for a decrease in S from 300 ppm to 11 ppm. It can be used at reduced pressure (3 MPa) with only a 15% decrease in hydrodesulfurization conversion as compared to the operation at 5 MPa.

1. Introduction

Strict environmental regulations on the sulfur content in fuels along with the poorer quality of the upgraded feedstock have reinvigorated considerable interest in deep hydrodesulfurization (HDS) technologies. As an example, Environment Canada—Air limits the maximum level of sulfur to 30 ppm in gasoline and 15 ppm in diesel fuel [1,2], which are now referred to as low-sulfur and ultra-low sulfur fuels. Sulfur reduction to such levels has to do primarily with the elimination of refractory sulfurous compounds such as dialkyl-dibenzothiophenes with alkyl groups adjacent to the sulfur atom, which makes the HDS process quite challenging [3]. 4,6-Dimethyldibenzothiophene (4,6-DMDBT) is a typical molecule in this category and is usually selected as a model compound for deep HDS studies [4].

Numerous works have been published on the HDS mechanism of dibenzothiophene (DBT) and its alkyl-substituted derivatives such as 4,6-DMDBT [5–10], which propose two major pathways for their HDS: (i) direct desulfurization (DDS), the path of lower hydrogen consumption achieved by the hydrogenolysis of the C—S bond of the reactant leading to the formation of sulfur-free aromatic products, and (ii) hydrogenation (HYD), the path that strongly relies on the availability of hydrogen initially to hydrogenate an aromatic ring of the sulfurous molecule before the C—S bond breakage, resulting in a mixture of sulfur-free aromatic and/or saturated rings (depending on the extent of hydrogenation). The DDS route requires the perpendicular adsorption of the reactant on the catalyst surface (σ mode), while HYD proceeds via the parallel bonding of the reactant with the surface (π mode) [4,5,11]. DDS is dominant for dibenzothiophene hydrotreating (80–90%) [12], but the HDS of 4,6-DMDBT mainly takes place through the HYD path, as the presence of methyl groups near the sulfur atom results in steric hindrance and prevents the perpendicular adsorption [3,11–13]. The steric change that occurs in the plane of a hydrogenated ring as compared to the remaining aromatic ring(s) reduces the hindrance imposed by the alkyl substitution [11]. Thus, it is suggested that a good hydrogenation catalyst is required for the deep HDS of 4,6-DMDBT [14].

Transition-metal supported catalysts, primarily based on Co/Mo and Ni/Mo, have been conventionally used for HDS [10,13,15–23], however, they are not active enough for acceptable levels of refractory compound desulfurization. It is suggested either that the catalyst volume must be increased several fold or that higher pressures are required, which is technologically challenging [24,25]. There is also a reported precedent of 85% DDS selectivity over phosphide catalysts of $NiFeP/SiO_2$ (at 30 atm and 340 °C) [26], but due to the low volumetric activity, reactor volumes must be increased several times to achieve comparable conversions with the existing Ni/Mo catalyst. Improved NiMo and CoMo catalysts have been marketed for ultra-deep desulfurization. As an example, a SMART

* Corresponding author.
E-mail address: semagina@ualberta.ca (N. Semagina).

http://dx.doi.org/10.1016/j.apcatb.2016.03.023
0926-3373/

Table 1
Characteristics of the studied catalysts.

Catalyst, support: γ-Al_2O_3	Pd/Ir loadings[a], wt.%	Colloidal particle size, nm	CO uptake, $mol_{CO}/mol_{(Pd+Ir)}$	Pd/Ir molar ratio	Particle size[b], nm
Pd	0.305/0.0	2.5 ± 0.4 [44]	0.04	–	17.2
$Pd_{8.8}Ir$	0.233/0.047	–	0.07	8.8	9.5
$Pd_{7.2}Ir_2$	0.259/0.131	2.9 ± 0.5	0.22	3.6	3.4
$Pd_{3.6}Ir$	0.181/0.090	2.6 ± 0.6	0.12	3.6	6.3
Pd_3Ir_2	0.185/0.225	–	0.16	1.5	5.2
$Pd_{1.4}Ir$	0.080/0.107	2.5 ± 0.6	0.18	1.4	4.6
Ir	0.0/0.231	1.5 ± 0.2 [44]	0.67	0.0	1.9

[a] Determined from NAA.
[b] Based on CO chemisorption and CO/metal surface ratio of 1.

catalyst is able to desulfurize dibenzothiophenes via DDS on its CoMo component and via hydrogenation on its NiMo component followed by hydrogenolysis [12]. Co/Mo catalysts are used at lower pressures than those of conventional HDS because they promote the DDS pathway [12].

An alternative solution is to add a second-stage hydrotreater with more active noble metal catalysts for ultra-deep desulfurization of initially pretreated fuels with 250–300 ppm S [27], which are largely composed of the most refractory molecules such as 4,6-DMDBT. In this scenario, the major emphasis for HDS of refractory sulfur compounds has been placed on promoted noble metal catalysts (Pt group) because of their high hydrogenation activity. The available literature on the use of noble metals for the HDS of 4,6-DMDBT is not very rich, and the existing works are almost exclusively limited to mono- and bimetallic Pd- and Pt-based catalysts [4,14,23,27–32]. In the HDS of DBT on supported Pd catalysts, DDS selectivity values are around 80% on Pd catalysts at conversion levels above 50% [23,33]. This is attributed to the lower activation energy in the DDS path of DBT [23]. However, in the case of 4,6-DMDBT, the steric hindrance of the methyl groups adjacent to the sulfur atom dramatically reduces the contribution of the DDS route on monometallic Pd catalysts, and the catalytic activity dominantly relies on the hydrogenation path. For instance, in a series of 4,6-DMDBT HDS studies performed on supported Pd catalysts [4,14,29], the DDS selectivity values were always found to be around 1% at various conversion levels.

From the capex and opex perspectives, it is desirable to shift the HDS mechanism toward the DDS path that does not require pressures as high as those needed for the hydrogenation path. Since DDS operates through hydrogenolysis, a catalyst with a high hydrogenolysis activity is required to make an impact in the DDS route. As has been shown for thiophene HDS on Pt [34] and Ru clusters [35], when thiophene binds onto sulfur vacancies by σ-bonding through the lone pair in the S-atom (η^1(S)-coordinated thiophene), desulfurization occurs, while its π-bonding through the aromatic ring (η^4-coordinated thiophene) results in hydrogenation. Small Pt clusters exhibit a greater preference for desulfurization due to the prevalence of coordinatively unsaturated edge and corner atoms, which bind with S more strongly and lead to lower metal availability and to a preference for η^1(S)-coordinated thiophene [34]. Thus, a first requirement for an efficient direct desulfurization route is smaller metal nanoparticles. This requirement makes the choice of Pd-only systems rather undesirable because of palladium's low resistance to thermal sintering. Recall that the presence of Pd should be especially desirable for 4,6-DMDBT HDS because its high hydrogenation ability may provide high formation rates of sulfurous hydrogenated intermediates with a weakened steric hindrance of the C—S bond to reach the catalyst surface.

A second metal may improve the sintering resistance of Pd, and, preferably, it should have a high hydrogenolysis activity. A lesson could be adopted from a ring-opening catalysis of naphthenic molecules, which occurs on a metal function either via a dicarbene mechanism, which occurs through the metal-carbon bonding of two carbon atoms standing perpendicular on the metal surface, or via a π-adsorbed olefin mode with flat reactant adsorption [36]. Among different noble metals, iridium reportedly displays the strongest tendency for ring opening via a dicarbene mechanism, and it is known in refineries for its outstanding hydrogenolysis activity [37–40]. Iridium forms a part of reforming Pt-Ir catalysts, which were introduced by Exxon in the 1970s with improved activity as compared to monometallic Pt, which had previously been used in commercial contexts [37].

In terms of HDS, the literature reports the removal of sulfur with Ir catalysts on smaller model molecules [41,42] as well as on real feed [39], but not on 4,6-DMDBT specifically. For instance, an Ir/MgF_2-MgO catalyst presented almost 50 times higher activity than a commercial Co/Mo catalyst in the HDS of thiophene [42]. The high DDS selectivity of Ir (~90%) has been reported in the HDS of DBT over a series of noble metal (Pt, Pd, Ru, and Ir) catalysts supported on zeolite HY [33,43]. However, studies of Ir in the HDS of a mixed feed or of molecules with a non-hindered C—S group do not provide information on how Ir's outstanding hydrogenolysis activity could be useful for the HDS of refractory sulfur compounds. To the best of our knowledge, no information is available for the Ir-catalyzed HDS of 4,6-DMDBT, in neither monometallic nor bimetallic formulations.

The research hypothesis of this work is that the iridium addition to palladium catalysts for 4,6-DMDBT HDS may improve the contribution of the C—S hydrogenolysis in both the parent DMDBT and the partly hydrogenated sulfurous intermediates formed in the hydrogenation route catalyzed by Pd. Iridium may bring about the advantages of an outstanding ring-opening catalyst for C—S bond cleavage. It may also improve the thermal resistance of sintering-prone palladium, thus decreasing the metal cluster size and contributing to a larger proportion of η^1(S)-coordinated intermediates. This is a first report on a noble metal catalyst development that takes advantage of metals with two different functionalities in order to promote both the HYD and DDS routes in 4,6-DMDBT HDS.

2. Experimental

2.1. Materials

$H_2IrCl_6{\cdot}xH_2O$ and H_2PdCl_4 were used as metallic precursors. Poly-vinylpyrrolidone (PVP, average MW: 40,000) was used as a stabilizing agent and γ-Al_2O_3 powder (150 mesh) with an average pore size of 58 Å and an SSA of 155 m^2/g (provided by the manufacturer) was used as a support material; these materials were obtained from Sigma-Aldrich. Ethanol and acetone were used as received from Fisher Scientific. Milli-Q water was used as a solvent and for washing the synthesis flasks. All of the gases were ultra-high purity (i.e. 99.999%) and purchased from Praxair. For catalytic reactions, *n*-decane (99.4%) from Fisher Scientific as well as *n*-dodecane (≥99%), indane (95%), and 4,6-dimethyldibenzothiophene (97%) from Sigma-Aldrich were used as received.

2.2. Catalyst synthesis and characterization

Mono- and bimetallic Pd and Ir nanoparticles were synthesized by colloid chemistry techniques in an ethanol-water solvent using PVP as a stabilizer (PVP/metal molar ratio of 5), deposited on γ-Al_2O_3 powder using acetone, and then calcined for 2 h at 400 °C in air to remove the polymeric stabilizer. The details of this process have been explained previously [40]. A simultaneous reduction of both metal precursors was used to synthesize $Pd_{8.8}Ir$, $Pd_{3.6}Ir$, $Pd_{1.4}Ir$, and Pd_3Ir_2. The $Pd_{7.2}Ir_2$ catalyst was synthesized via a hydrogen-sacrificial technique: PVP-stabilized Pd nanoparticles (PVP/metals molar ratio of 5/1) were treated with H_2 for 1.5 h to form hydride species on their surface, and these were subsequently replaced by Ir atoms forming a shell around Pd core particles, as has been explained previously [40].

Neutron activation analysis (NAA), temperature-programmed reduction (TPR), transmission electron microscopy (TEM), and the pulse chemisorption of CO were performed as has been described previously using AutoChem 2950HP device (Micromeritics, USA) [44]. The analyses were done on samples calcined and reduced in hydrogen at 400 °C. This treatment ensures the complete removal of PVP residues from a catalytic surface [44]. Temperature-programmed reduction (TPR) analysis of the supported catalysts was also studied on AutoChem 2950HP device. The TPR was performed on samples pre-calcined at 400 °C with a mixture of 10% H_2 in Ar from room temperature to 400 °C with a heating rate of 10 °C/min.

Elemental analysis for the S content of a spent catalyst was performed with an Elementar Vario Micro elemental analyzer on a bimetallic sample, $Pd_{7.2}Ir_2$, after a 3-day HDS stability test followed by purging in an inert medium.

Diffuse reflectance infrared Fourier transform spectroscopy (DRIFTS) of adsorbed pyridine was performed with a Nicolet Nexus670 spectrophotometer in the range of 800–3000 cm^{-1}, averaging over 128 scans. Calcined samples (2 h in air at 400 °C) were reduced in a fixed-bed reactor under hydrogen at 375 °C and kept for 1 h, followed by cooling down to the ambient temperature in the same atmosphere. Nitrogen saturated with pyridine was passed through the samples for 1 h, the details of this process can be found elsewhere [44]. The samples were purged with pure nitrogen for 30 min at 100 °C to desorb the physisorbed pyridine and the DRIFTS spectra were recorded immediately. An overnight-dried potassium bromide (KBr) from Sigma-Aldrich was used to collect the background spectra dilute the samples. One blank analysis was also performed on calcined γ-Al_2O_3 without pyridine treatment. OMNIC software was used to transform the reflectance spectra to Kubelka-Munk units.

The specific surface area and the pore size distribution of the support material (γ-Al_2O_3 powder) were collected by nitrogen adsorption-desorption isotherms using a Quantachrome Autosorb 1 MP analyzer at 77.3 K. The Brunauer–Emmett–Teller (BET) method was used for the calculation of the specific surface area followed by the Barrett–Joyner–Halenda (BJH) technique for the determination of pore size distribution.

Other characterization methods including X-ray photoelectron spectroscopy (XPS), ion-scattering spectroscopy (ISS), X-ray absorption near-edge structure (XANES) and diffuse reflectance infrared Fourier transform spectroscopy (DRIFTS) of adsorbed carbon monoxide (CO) have previously been used to study the structure of these types of bimetallic catalysts in more detail [40,44], and thus they have not been repeated here. However, a brief summary of their results is provided in Section 3.1.

Table 1 summarizes the characteristics of the synthesized catalysts. Note that the catalyst abbreviations (for example, $Pd_{8.8}Ir$) refer to the molar ratio of the metals in the final catalysts, as determined by neutron activation analysis (NAA) and does not necessarily reflect the phase composition.

2.3. Catalytic experiments: 4,6-DMDBT hydrodesulfurization

The catalytic tests were performed in a continuous fixed-bed reactor of 22″ length and ½″ i.d. The supported catalysts were activated by in-situ reduction at 300 °C for 1 h before the reaction. All of the HDS reactions were studied after an overnight (15 h) stabilization period at reaction conditions. Liquid samples were collected every 2 h after the stabilization period. A difference in conversion of only 2–3% was observed after the second sample (i.e., 17 h on stream), indicating that a steady-state condition was established after the stabilization period. The setup and the method were adapted from the reported works on HDS of 4,6-DMDBT [23] and were confirmed here to ensure that the system had reached a steady state and that the collected samples were representative of the data point's conditions. A second condenser was used parallel to the first one in order to prevent pressure fluctuations and instability at the time of sampling.

The initial activity evaluation in 4,6-DMDBT HDS was performed at 300 °C and 5 MPa using 0.09 g of the supported catalysts diluted with about 4 g of #100 mesh SiC. A mixture of 0.5 wt.% 4,6-DMDBT (about 800 ppmw S) and 3.5 wt.% dodecane (internal standard) balanced with *n*-decane (as solvent) was fed to the top of the reactor by a Series II high pressure pump (0.05 cc/min), where it was mixed with hydrogen (100 cc/min) at a H_2/liquid ratio of 16 mol/mol and WHSV = 24 h^{-1} (based on liquid). The phase calculations predict that DMDBT at such conditions should be fully vaporized. The reaction conditions were varied as will be discussed in Section 3.

The collected liquid samples were analyzed off-line using a Varian 430 gas chromatogram (GC) equipped with a CP-Sil 8CB Varian capillary column (50 m length and 0.25 mm inner

Table 2
Catalytic performance of the bimetallic catalysts in 4,6-DMDBT hydrodesulfurization at 300 °C, 5 MPa, 800 ppm S in the feed and liquid WHSV of 24 h^{-1} using 0.09 g of the metal supported catalysts.

Catalyst	DMDBT conversion (%)	Activity, 10^{-3} $mol_{DMDBT}/mol_{Pd+Ir}/s$	Surface activity, 10^{-3} $mol_{DMDBT}/mol_{adsorbedCO}/s$[b]	Selectivity (%)				
				S-free products	S-free products via HYD	HYD path	DDS path	HYD/DDS
Pd	34	2.1	53	38	34	95	5	20.3
$Pd_{8.8}Ir$	47	3.3	47	88	75	87	13	6.8
$Pd_{3.6}Ir$	40	3.2	27	91	79	88	12	7.5
Pd_3Ir_2[a]	36	4.3	27	93	63	70	30	2.3
$Pd_{1.4}Ir$	35	4.7	26	93	67	74	26	2.8
Ir	15	2.2	3	67	36	69	31	2.2

[a] 0.045 g of this catalyst was used to study the mass transfer limitations with Madon–Boudart test.
[b] "Mole of adsorbed CO" should not to be confused with the number of surface atoms because Ir and Pd exhibit different stoichiometry for CO adsorption, i.e., between 1 and 2 for CO/Ir [47] and 0.6 for CO/Pd [48].

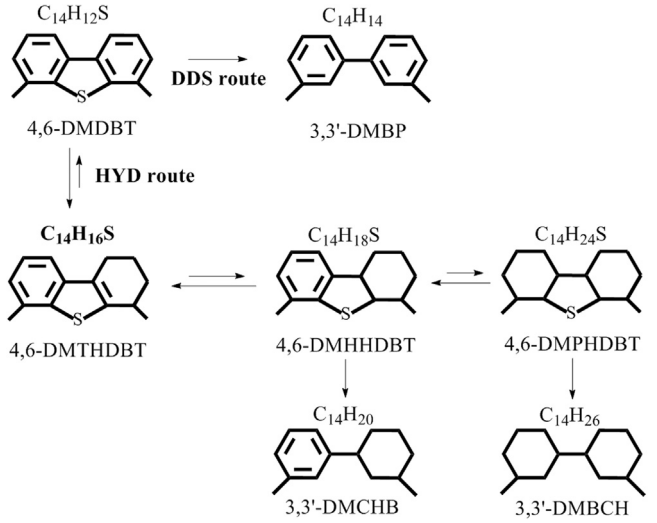

Scheme 1. The DDS and HYD reaction pathways in the HDS of 4,6-DMDBT at 300 °C and 5 MPa. Reprinted from [23] with permission from Elsevier.

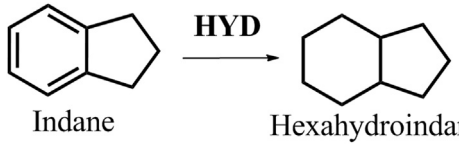

Scheme 2. The hydrogenation (HYD) of benzocyclopentane (indane) at 300 °C and 5 MPa.

diameter) and a flame ionization detector (FID). The oven was heated with a ramping rate of 10 °C/min to 300 °C, which allowed for the clear separation of the reactant as well as the reaction products. Various peaks were observed, which agreed with the results reported in the literature [23] (also confirmed by GC–MS): 3,3′-dimethylbicyclohexyl (3,3′-DMBCH) and 3,3′-dimethylcyclohexylbenzene (3,3′-DMCHB) as the desulfurized products of the hydrogenation (HYD) path; 3,3′-dimethylbiphenyl (3,3′-DMBP) as the final product of the direct desulfurization path (DDS); and 4,6-dimethyltetrahydrodibenzothiophene (4,6-DMTHDBT), 4,6-dimethylhexahydrodibenzothiophene (4,6-DMHHDBT), and 4,6 dimethylperhydrodibenzothiophene (4,6-DMPHDBT) as the sulfurous intermediates in the HYD path, which are shown in Scheme 1 [23].

The quantification of the GC areas was completed by analyzing calibration mixtures containing *n*-decane, dodecane (as an internal standard), 4,6-DMDBT, and 3,3′-DMBP. Five calibration mixtures with different concentrations of 4,6-DMDBT and 3,3′-DMBP were used so that the calibrating lines covered the whole range of conversions. Sulfur-containing intermediates were quantified similarly to 4,6-DMDBT, and the sulfur-free products were treated the same as 3,3′-DMBP due to structural similarity.

The absence of external and internal mass transfer limitations was verified with a Madon–Boudart test [45]. For this purpose, the bimetallic sample Pd_3Ir_2 was prepared with a similar Pd/Ir molar ratio as that of $Pd_{1.4}Ir$ but with twice the loading of both metals. The CO uptake of this sample presented in Table 1 is close to that of $Pd_{1.4}Ir$ (0.16 vs. 0.18 $mol_{CO}/mol_{(Pd+Ir)}$), indicating a similar dispersion for both samples. The activity values are identical (Table 2: 26 and 27×10^{-3} $mol_{DMDBT}/mol_{surface(Pd+Ir)}/s$) and manifest the absence of mass transfer limitations. The heat transfer limitations were not verified, but they were assumed negligible because of low metal loading (0.3 wt.%) and bed dilution with inert SiC (~0.1 g catalyst diluted with 4 g of SiC).

A blank run with pure γ-Al_2O_3 diluted with SiC showed a negligible activity of the support (below 2% conversion), implying the necessity of metallic centers for catalytic activity.

The following terms are used in the analysis of the results (molar basis):

- DMDBT conversion: the amount of 4,6-DMDBT converted during the HDS reaction divided by the initial amount of 4,6-DMDBT in the feed;
- HDS conversion: the total amount of sulfur removed by the HDS reaction divided by the initial amount of sulfur in the feed (as 4,6-DMDBT);
- Activity: the DMDBT conversion multiplied by the entering molar flow rate of the DMDBT divided by the total mole of the metals in the catalyst used (or surface atoms, when so specified);
- Selectivity to sulfur-free products: the amount of sulfur-free products (i.e., DMBCH, DMCHB, and DMBP) divided by the amount of 4,6-DMDBT converted;
- Selectivity to sulfurous intermediates: the amount of sulfur-containing intermediates (i.e., DMTHDBT, DMHHDBT, and DMPHDBT) divided by the amount of 4,6-DMDBT converted;
- Selectivity to the DDS path: the amount of DMBP divided by the amount of 4,6-DMDBT converted;
- Selectivity to the HYD path: the collective amount of DMBCH, DMCHB, DMTHDBT, DMHHDBT, and DMPHDBT divided by the amount of 4,6-DMDBT converted;
- Selectivity to S-free products in the HYD path: the amount of DMBCH and DMCHB divided by the amount of 4,6-DMDBT converted.

2.4. Catalytic experiments: indane (benzocyclopentane) hydrogenation

The high-pressure hydrogenation of indane was studied with the same fixed-bed system as described above using 0.32 g of the selected supported catalysts diluted with SiC. A mixture containing 2 wt.% indane and 2 wt.% dodecane (as internal standard) balanced with *n*-decane was pumped to the system. The reactions were studied at 5 MPa and 300 °C after a stabilization period of 15 h at the reaction conditions. Relatively harsh operating conditions were used for these reactions corresponding to the liquid flow of 0.3 cc/min and H_2/liquid ratio of 4 mol/mol (liquid WHSV = 41 h^{-1}). The liquid samples were analyzed with the same GC explained above. To separate the main reaction product, i.e. hexahydroindane, from *n*-decane, a 40-min isothermal program at 75 °C was used. Ring-opening products, i.e., *n*-propylcyclohexane, ethylcyclohexane, and methylcyclohexane, were detected but in negligible amounts at the conditions studied (less than 1 mol% in total). γ-Al_2O_3 diluted with SiC did not show indane conversion.

The high-pressure hydrogenation of indane was also studied in the presence of 300 ppm S as 4,6-DMDBT at 5 MPa, 300 °C, and 0.32 g of the catalyst. The performance was evaluated after an overnight (15 h) stabilization period. Two operating conditions were also studied over 72 h: (i) H_2/liquid = 16 mol/mol, liquid WHSV = 7 h^{-1} (referred as light conditions), and (ii) H_2/liquid = 4 mol/mol, liquid WHSV = 41 h^{-1} (referred as harsh conditions).

The carbon balance deviation in all of the above-mentioned reactions was in the range of 5%.

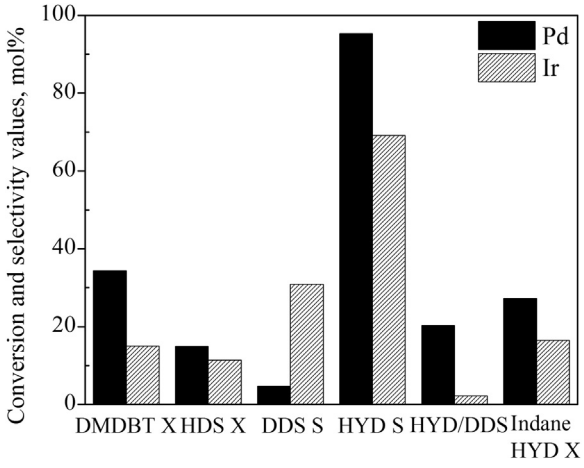

Fig. 1. Comparison of Pd/γ-Al_2O_3 and Ir/γ-Al_2O_3 performance at 300 °C and 5 MPa, 800 ppm S in the feed, liquid WHSV: 24 h^{-1}: 4,6-DMDBT conversion (DMDBT X), HDS conversion (HDS X), selectivity to DMBP (DDS S), hydrogenation route selectivity (HYD S) and ratio of HYD and DDS selectivities (HYD/DDS), as well as in sulfur-free benzocyclopentane (indane) hydrogenation (Indane HYD X).

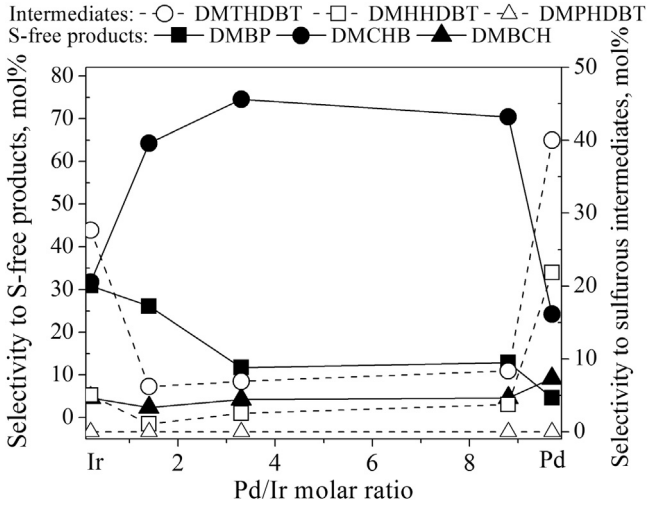

Fig. 2. Selectivities as a function of Pd/Ir molar ratio in the bimetallic catalysts at 40 ± 7% DMDBT conversion (except for 15% for Ir) at 300 °C, 5 MPa, 800 ppm S in the liquid feed, liquid WHSV: 24 h^{-1}.

3. Results and discussion

3.1. Ir serves as a hydrogenolysis co-metal and a structural promoter to a hydrogenating Pd in HDS of 4,6-DMDBT

3.1.1. Catalytic properties

Pd and Ir catalysts (0.305 wt.% and 0.231 wt.% respectively loaded on γ-Al_2O_3) exhibited similar 11–15% sulfur removal from a 4,6-DMDBT feed (800 ppm S), but the Pd catalyst was almost twice as active in 4,6-DMDBT conversion. As opposed to Ir, the Pd catalyst exhibited a preferential formation of sulfurous intermediates via the hydrogenation path as well as a lower contribution from C—S bond hydrogenolysis. As seen from Fig. 1, selectivity to DMBP (product of the direct desulfurization path) was 31% for Ir vs. 5% for Pd, though with the same extent of overall S removal. The ratio of all products in the HYD path to the DDS path was 10 times higher for Pd than for Ir. These findings are in line with the expected trend [4,14]: Pd is a known active hydrogenation catalyst and is expected to perform sulfur removal mostly via the hydrogenation path, while Ir performs an efficient hydrogenolysis [33,38,39].

To evaluate the extent of the sulfur poisoning during 4–6 DMDBT HDS, we performed S-free hydrogenation of benzocyclopentane (indane, Scheme 2) under the same conditions of 300 °C and 5 MPa. Only a fully hydrogenated product was observed, without any contribution from cracking. Again, Pd was more active than Ir. Most important is that the ratio of conversions in the hydrogenation of the S-free feed (Fig. 1) and the ratio of selectivities in the HYD path with 800 ppm S in the feed (Table 2) was similar, i.e., 1.5 ± 0.1 (Pd/Ir). This indicates that the sulfur's influence on the HYD route in the 4,6-DMDBT HDS is the same for Pd and Ir and that the difference in the metals' HDS performance is connected not to a selective sulfur poisoning of HYD sites on Ir or Pd, but to the involvement of the C—S hydrogenolysis active sites of iridium. Such a finding is not surprising: the ratio of partial pressures $p(H_2S)/p(H_2)$ in the gas mixture in equilibrium with solid sulfides at 600 K is similar for PdS and IrS_2 on the order of 10^{-2} [46].

The bimetallic Pd-Ir catalysts exhibited 3–4-fold higher HDS activities as compared to monometallic Pd. Table 2 and Fig. 2 reveal the beneficial effects of adding Ir to Pd as a function of the Pd/Ir molar ratio. At 40 ± 7% DMDBT conversions, the selectivity to S-free products improved up to 93% upon the addition of Ir as compared to 38% for monometallic Pd. The selectivity to the DDS path for the Ir-containing catalysts increased up to 26% versus 5% for the Pd-only catalyst. The DMBP selectivity increases as the amount of Ir increases, but it does not surpass the value for Ir alone (31% at 15% DMDBT conversion). However, the selectivity to DMCHB (S-free product via the HYD path) almost triples at a Pd/Ir ratio of approximately 4 versus monometallic Pd. The steric hindrance for C—S bond cleavage in the preceding sulfurous intermediate DMHHDBT (Scheme 1) is lessened as compared to the parent DMDBT. The co-existence of Pd and Ir provides a synergistic effect: Ir alone cannot hydrogenate DMDBT as effectively as Pd, but it ensures the improved C—S cleavage of the sulfurous intermediates obtained through hydrogenation on Pd. In the hydrogenation path, the presence of Pd proved beneficial by supplying hydrogenated sulfurous intermediates to Ir for the cleavage. As seen in Table 2, HYD/DDS path selectivity ratios decrease from 20 to 2 as the Ir content in the catalysts increases.

However, the observed synergism is not only due to the intrinsic propensity of Pd for hydrogenation and Ir for hydrogenolysis. Although no kinetic studies under differential conditions were performed to evaluate intrinsic turnover frequencies, the activity values expressed in terms of converted 4,6-DMDBT over moles of adsorbed CO (from CO chemisorption) at similar 40 ± 7% conversions were the highest for monometallic Pd and the bimetallic $Pd_{8.8}Ir$ (52×10^{-3} and 47×10^{-3} $mol_{DMDBT}/mol_{adsorbedCO}/s$), followed by $Pd_{3.6}Ir$ and $Pd_{1.4}Ir$ (27 and 6×10^{-3} $mol_{DMDBT}/mol_{adsorbedCO}/s$). The same value for the 15% DMDBT conversion over monometallic Ir was only 3×10^{-3} $mol_{DMDBT}/mol_{adsorbedCO}/s$. Note that "mole of adsorbed CO" should not to be confused with the number of surface atoms because Ir and Pd exhibit different stoichiometry for CO adsorption, i.e., 1–2 for CO/Ir [47] and to 0.6 for CO/Pd [48]. The activity values are not turnover frequencies and are shown only as a trend of the surface activity: monometallic Pd is the most active, Ir is the least active, and the bimetallic catalysts show intermediates activities. Thus, the observed low activity of monometallic Pd catalyst is due to its low resistance to sintering, with its highest surface activity converting 4,6-DMDBT mainly through the hydrogenation path.

Thus, in 4,6-DMDBT HDS, Ir serves both as a textural promoter to improve metal dispersion as well as a second functional component for enhanced hydrogenolysis of the hydrogenated intermediates. This experimental finding is in line with the proposed research hypothesis that Ir brought about the advantage of an outstanding ring-opening catalyst for C—S bond cleavage because of preferred perpendicular adsorption via the σ-mode. Iridium also improved

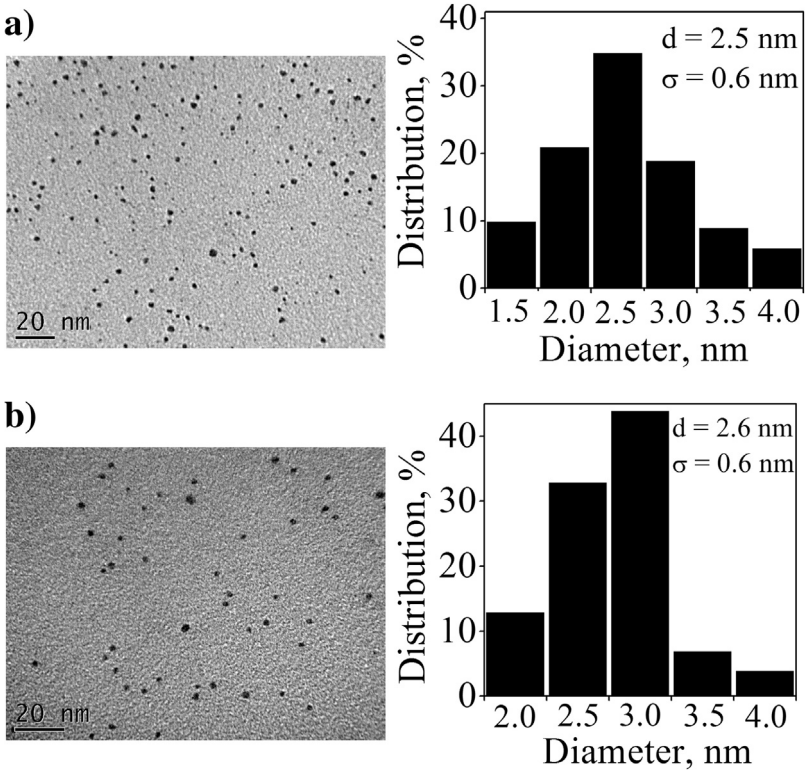

Fig. 3. TEM images of $Pd_{1.4}Ir$ (a) and $Pd_{3.6}Ir$ (b) colloidal bimetallic nanoparticles synthesized by the polyol technique (PVP/metal molar ratio: 5/1).

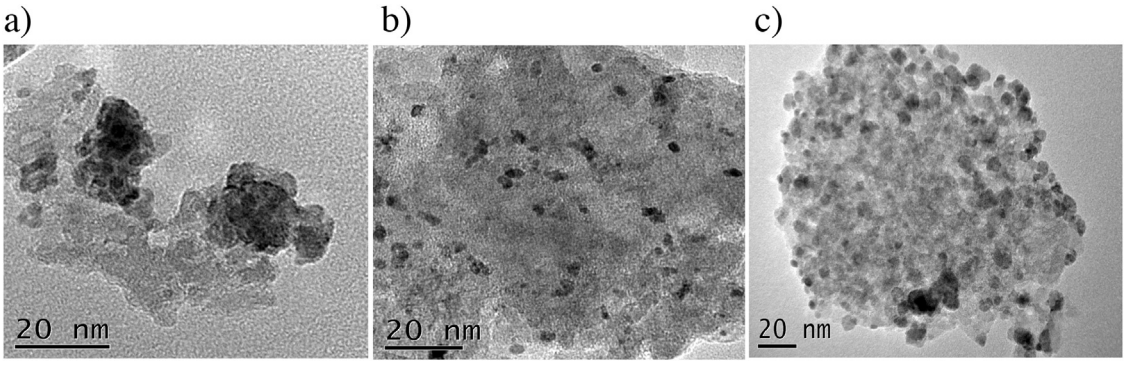

Fig. 4. TEM images of Pd (a), Ir (b) and $Pd_{7.2}Ir_2$ (c) catalysts after 2 h calcination at 400 °C.

thermal resistance of sintering-prone palladium and decreased the metal cluster size, which contributed to the larger proportion of η^1(S)-coordinated intermediates.

The elemental sulfur analysis performed on Pd7.2Ir2 catalyst after one day on stream with 800 ppm S in the feed was found to be 0.15 wt.% S content in the catalyst and indicated metal sulfidation. An exemplary $Pd_{7.2}It_2$ bimetallic catalyst allowed for sulfur removal from 300 ppm to 11 ppm at 300 °C, 5 MPa, liquid WHSV of 12 h^{-1} and hydrogen/liquid feed molar ratio of 16.

3.1.2. Characterization results to support textural and chemical synergism in the bimetallic samples

As seen in Table 1, the addition of Ir to Pd significantly improves metal dispersion. Ir also serves as a textural, anti-sintering promoter for Pd. The size of colloidal monometallic and bimetallic nanoparticles was in the range of 1.5–3.0 nm depending on the composition (Table 1 and Fig. 3), but after the thermal treatment for polymer removal and catalyst conditioning in hydrogen before HDS, only the Ir-rich samples demonstrated high dispersion as evidenced by CO chemisorption (Table 1) and TEM images (Fig. 4), with monometallic Pd being the least sintering-resistant sample.

The absence of large Pd agglomerates, that are characteristic of the monometallic Pd, evidences the intrinsic bimetallic nature of the catalyst when two metals are alloyed in one nanoparticle instead of a physical mixture of two monometallic particles. In accordance with such bimetallicity, the temperature-programmed reduction (TPR) of the $Pd_{1.4}Ir$ catalyst (Fig. 5) does not demonstrate the characteristic feature of Pd (low-temperature decomposition of Pd hydride) that is present in the physical mixture of Pd and Ir nanoparticles. The TPR of the physical mixture of the monometallic Pd and Ir catalysts merely shows the overlap of monometallic Pd and monometallic Ir, i.e. featuring the negative, low-temperature peak of Pd due to Pd-β hydride decomposition [49] as well as the two peaks for Ir oxide reduction at 200 and 275 °C [50]. In contrast, the TPR of an exemplary bimetallic catalyst, i.e. $Pd_{1.4}Ir$, shows the profile of a new cluster without any negative peaks below 100 °C, as well as two peaks similar to monometallic Ir but at lower

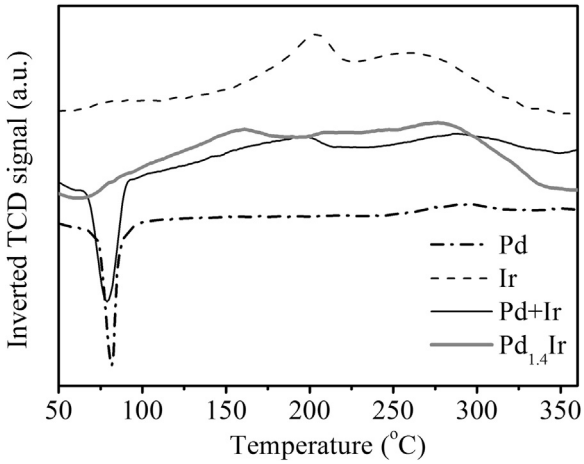

Fig. 5. TPR profiles of Pd, Ir, $Pd_{1.4}Ir$ and the physical mixture of Pd and Ir (Pd + Ir) supported catalysts (the negative signal indicates hydrogen evolution).

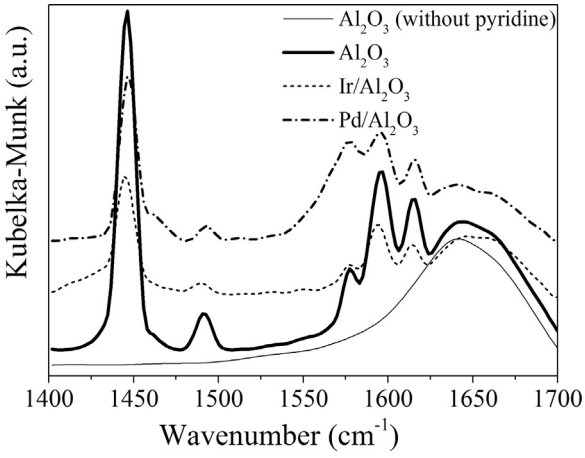

Fig. 6. DRIFT spectra of adsorbed pyridine on γ-Al_2O_3 and selected γ-Al_2O_3-supported catalysts.

temperatures of 180 and 260 °C, respectively, which indicates chemical synergism between the two metals.

In addition to the TPR results mentioned here, these types of bimetallic Pd-Ir catalysts supported on γ-Al_2O_3 have been extensively characterized in our recent papers to verify the bimetallic interactions as well as their surface structures [40,44]. Briefly, X-ray photoelectron spectroscopy (XPS), ion-scattering spectroscopy (ISS), and X-ray absorption near-edge structure (XANES) confirmed the presence of electronic interactions between Pd and Ir atoms in the bimetallic structure.

Also, the results of ISS, XANES, and DRIFTS of adsorbed carbon monoxide (CO-DRIFTS) showed that the Pd-Ir samples prepared via simultaneous reduction (such as the samples in this work, apart from $Pd_{7.2}Ir_2$) exhibited mixed surfaces with coexistent Pd and Ir atoms, while the Pd(core)-Ir(shell) samples (similar to the current $Pd_{7.2}Ir_2$) exposed excess iridium atoms on the surface. The spectra and characterization results have been reported previously [40,44].

The catalyst support activity in a blank HDS test was found negligible and no solid-acid-catalyzed isomerization products were detected. The surface acidity of γ-Al_2O_3 as well as monometallic Pd- and Ir-supported catalysts were studied by the DRIFT spectroscopy of adsorbed pyridine in the range of 1400–1700 cm^{-1} and presented in Fig. 6. Five peaks were observed for γ-Al_2O_3 at 1446, 1490, 1578, 1596, and 1615 cm^{-1}, respectively, which agreed with

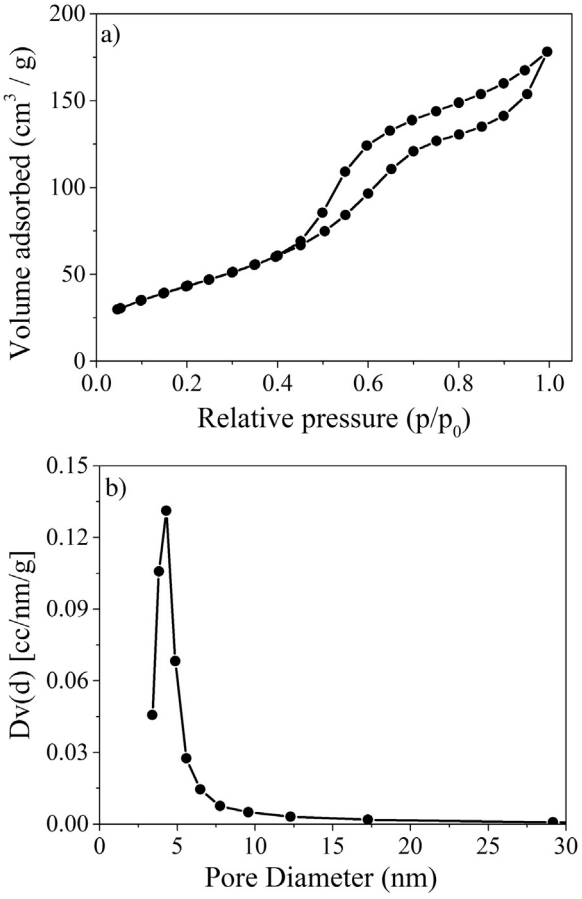

Fig. 7. Nitrogen adsorption-desorption isotherm (a) and pore size distribution profile (b) of γ-Al_2O_3 calcined in air at 400 °C.

the literature data regarding the presence of strong (1446 cm^{-1}), medium strong (1615 cm^{-1}), and weak Lewis acid sites (1578 and 1596 cm^{-1}) [51,52]. No adsorption band was discernible at about 1540 cm^{-1}, implying the absence of Brønsted acid sites [52]. The spectra for the supported monometallic Pd and Ir catalysts showed the same peak positions, suggesting that the presence of metals or the treatment of the deposited catalysts did not alter the surface acidity in a significant manner.

It is important to note that the discussed textural synergism may depend significantly on the choice of support. The dramatic dispersion enhancement of Pd upon the addition of Ir might be not so pronounced if smaller, monometallic Pd particles could be stabilized on a support. Such improved dispersions may occur at lower metal loading, higher support porosity, stronger metal-support interactions, methods of the active phase deposition, and catalyst treatment (such as drying speed or a sequence of oxidation/reduction treatments) [53–55]. A support with a pore size of 3–12 nm (maximum at 4.3 nm) and a BET surface area of 162 m^2/g (Fig. 7) was selected to accommodate the pre-synthesized colloidal nanoparticles of ca. 2.5 nm diameter. Typically, at such low Pd loadings as have been reported here (up to 0.4 wt.%), other γ-aluminas that have been impregnated with molecular Pd precursors may sustain Pd particles smaller than the 17 nm reported here (Table 1) because of more uniform distribution on the internal surface. In the current work, to differentiate the textural difference after the Ir addition, we intentionally selected a larger monometallic Pd particle size that decreased with the increasing proportion of Ir at the same total metal loading.

Table 3
Pressure effect in 4,6-DMDBT HDS at 300 °C, 0.18 g of $Pd_{7.2}Ir_2/\gamma$-Al_2O_3 catalyst, H_2/liquid: 16 mol/mol, 300 ppm S in the feed.

P, MPa	Liquid WHSV (h^{-1})	DMDBT X (%)	HDS X (%)	Selectivity values[a] (mol%)						
				DM-THDBT	DM-HHDBT	DMBP	DMCHB	DMBCH	HYD	HYD/DDS
3	12	89	87	0.9	0.4	25.7	68.3	4.6	74	2.9
	18	78	76	1.8	0.5	27.0	67.0	3.8	73	2.7
	24	72	70	2.0	0.8	28.1	65.7	3.3	72	2.6
5	12	98	98	0.3	<0.1	15.5	76.4	7.7	84	5.4
	18	92	91	0.7	0.5	16.7	76.0	6.0	83	5.0
	24	86	84	1.4	0.7	18.2	74.7	5.1	82	4.5

[a] DMPHDBT selectivity was below 0.1% in all runs.

Table 4
Effect of benzocyclopentane (indane) presence on 4,6-DMDBT HDS at 300 °C, 5 MPa for $Pd_{7.2}Ir_2/\gamma$-Al_2O_3 catalyst.

Sulfur-free hydrogenation of indane (W_{cat}: 0.32 g, H_2/liquid:4 mol/mol)

Liquid WHSV (h^{-1})	Indane X (%)	Selectivity to hexahydroindane (mol%)	Selectivity to ring opening products
41	96	>99	<1

HDS of 4,6-DMDBT (W_{cat}: 0.09 g, H_2/liquid:16 mol/mol, 300 ppm S)

Liquid WHSV (h^{-1})	DMDBT X (%)	HDS X (%)	Indane X (%)	Selectivity values (mol%)							
				DM-THDBT	DM-HHDBT	DM-PHDBT	DMBP	DMCHB	DMBCH	HYD	HYD/ DDS
36	76	74	–	1.9	0.6	<0.1	21.8	71.4	4.2	78	3.6
HDS of 4,6-DMDBT and HYD of indane (W_{cat}: 0.32 g, 300 ppm S)											
41	46	41.9	<0.1	11.9	2.7	0.7	19.3	61.9	3.4	81	4.2
7[a]	99	97	5	0.4	0.7	0.8	15.0	72.9	10.2	85	5.7

[a] H_2/Liquid: 4 mol/mol at liquid WHSV 7 h^{-1} and 16 mol/mol at liquid WHSV 41 h^{-1}.

3.2. Direct desulfurization selectivity enhancement by pressure decrease

The addition of Ir to Pd, as shown above, allows for an increase in the contribution of the direct desulfurization path to the total sulfur removal. Thermodynamically, the hydrogenation path can be enhanced by the process pressure increase, while the direct desulfurization path is not affected by the pressure because the same number of moles are consumed and produced in the DMBP formation (Scheme 1). Thus, the DDS/HYD selectivity ratio should increase with the pressure decrease. However, the pressure decrease may negatively affect the overall sulfur removal and 4,6-DMDBT consumption rate because the HDS mostly proceeds via the pressure-sensitive hydrogenation path. Thus, the pressure effect was addressed for a bimetallic Pd-Ir catalyst at 3 and 5 MPa and at different WHSVs. As seen in Table 3, indeed, at the reduced pressure, the HYD/DDS selectivity ratio decreased almost by half. The selectivity to DMBP increased from ~16% to ~27%. With the decreased pressure, as expected, DMTHDBT, DMCHB, and DMBCH production within the HYD route decreased. Most importantly, such a dramatic pressure reduction (from 5 to 3 MPa) resulted in only a 10–15% decreased HDS conversion.

It is generally considered [24,25] that, in order to convert refractory sulfur compounds (such as 4,6-DMDBT), a significant increase in operating pressure is required as compared with more easily desulfurized molecules (such as thiophene) so that the HYD path may be enhanced to lessen the steric hindrance during the parent molecule adsorption for S extraction. Our findings indicate that not only is the pressure increase required, but it could also be reduced when a catalyst with enhanced DDS route selectivity is used. In such a case, the conversion decrease is not concomitant with the pressure decrease: the 1.7-fold pressure decrease is accompanied by only a 1.1–1.2-fold decrease in sulfur removal.

3.3. HDS inhibition in benzocyclopentane presence

Since the industrial feeds also contain a variety of polycyclic aromatic and naphthenic hydrocarbons [56–58], we also evaluated the 4,6-DMDBT HDS in the presence of indane (benzocyclopentane), which can serve as a model compound for the competitive hydrogenolysis (ring opening) of a naphthenic ring and the hydrogenation of the aromatic ring. Depending on the reaction conditions, the hydrocarbon could either be hydrogenated, cracked, or remain intact during S removal from the refractory sulfur compound.

When 4,6-DMDBT was co-fed with benzocyclopentane (indane) at the same high WHSV levels, the DMDBT conversion decreased from 76 to 46% as opposed to the DMDBT-only feed (Table 4). Notably, the absolute values of selectivities in the HYD and DDS paths, as well as their ratios, were not affected by the presence of benzocyclopentane. Most likely, benzocyclopentane behaves as a non-selective poison adsorbing on both on DDS- and HYD-active sites. At the high WHSV, no indane conversion was observed in the presence of DMDBT (versus almost 100% conversion in S-free indane feed). Indane adsorption on the DDS and HYD active sites in the S feed is most likely too strong and does not yield a hydrogenated indane: in the case of weak adsorption, no DMDBT rate suppression would have been observed. When the WHSV level was lowered and an almost 100% DMDBT conversion was achieved (Table 4), insignificant (5% conversion) indane hydrogenation occurred. No cracking products of benzocyclopentane were observed at this pressure. Thus, the developed catalysts allowed for the efficient S removal from a refractory sulfur compound without hydrogenolysis or the cracking of the naphthenic or aromatic rings.

It is important to note that in ultra-low desulfurization technologies nitrogen—containing basic compounds are present in the feed at the similar levels as the residual sulfur and can inhibit HDS via competitive adsorption [59]. The effect, however, depends on the nature of the nitrogen molecule, as such, both 2-methylpyridine and 2-methylpiperidine suppressed the hydrogenation pathway of DBT HDS; 2-methylpyridine also inhibited the DDS but 2-methylpipiredine hardly influenced the DDS path [60]. This suggests that the nitrogen inhibition could be lessened for HDS with enhanced DDS path, as achieved in the current work. The hypothesis warrants that the bimetallic Pd-Ir catalysts developed

in this work must be further evaluated for the nitrogen inhibition effect.

4. Conclusions

The performed study took advantage of two metals with different functionalities in the HDS of a refractory sulfur compound: i.e., for the first time, Pd with high hydrogenation ability and Ir with outstanding ring opening (hydrogenolysis) activity were combined in one formulation to promote HYD and DDS routes, respectively, in 4,6-DMDBT hydrotreating.

The effect of adding Ir to Pd/γ-Al_2O_3 catalysts for the hydrodesulfurization of 4,6-DMDBT was studied for the feed with 300–800 ppm S at 300 °C and 5 and 3 MPa pressure. The catalysts allowed for a decrease in S from 300 ppm (4,6-DMDBT) to 11 ppm. At 40 ± 7% DMDBT conversions, the selectivity to S-free products improved up to 93% upon the addition of Ir as compared to 38% for monometallic Pd. The selectivity to the direct desulfurization path for the Ir-containing catalysts increased up to 26% versus 5% for the Pd-only catalyst. The enhancements were attributed to both textural synergism (Ir improves Pd resistance to sintering) and chemical synergism (Pd provides enhanced formation of semi-hydrogenated sulfurous intermediates followed by Ir-catalyzed hydrogenolysis of the C—S bond). When benzocyclopentane was co-present in the feed, it inhibited the HDS activity but remained intact or underwent insignificant hydrogenation at 5 MPa pressure. The Pd-Ir catalyst allowed for the decrease of the operating pressure from 5 to 3 MPa at only a 15% decrease of hydrodesulfurization conversion. This is because of the increased contribution of the direct desulfurization path at the reduced pressure.

The reported catalysts have low metal loadings that should be increased for possible applications. Our study aimed to understand the Pd and Ir metal functions in 4,6-DMDBT HDS. To ensure bimetallicity, we used colloidal techniques to synthesize our catalysts, which yielded low metal loadings. However, the study may pave the way to the development of ultra-deep desulfurization catalysts that are able to decrease the operating pressure because of the direct desulfurization pathway selectivity enhancement. The double-functionality system may be also suitable for other hydrotreating technologies that involve ring opening and hydrogenation.

Acknowledgements

Financial support from the Institute for Oil Sands Innovation at the University of Alberta is gratefully acknowledged (grant 2011-01). Dr. L. Wu, L. Dean, and W. Boddez contributed to the HDS setup development. Dr. J. Duke, Dr. X. Tan, and J. Bryska are acknowledged for performing NAA and CHNS analyses.

References

[1] http://www.ec.gc.ca/energie-energy/default.asp?lang=En&n=BEA13229-1.html, (accessed 28.08.15.).
[2] http://www.ec.gc.ca/energie-energy/default.asp?lang=En&n=7A8F92ED-1.html, (accessed 28.08.15.).
[3] S.K. Bej, S.K. Maity, U.T. Turaga, Energy Fuels 18 (2004) 1227–1237.
[4] A. Röthlisberger, R. Prins, J. Catal. 235 (2005) 229–240.
[5] M. Houalla, D.H. Broderick, A.V. Sapre, N.K. Nag, V.H.J. de Beer, B.C. Gates, H. Kwart, J. Catal. 61 (1980) 523–527.
[6] M.J. Girgis, B.C. Gates, Ind. Eng. Chem. Res. 30 (1991) 2021–2058.
[7] P.T. Vasudevan, J.L.G. Fierro, Catal. Rev. Sci. Eng. 38 (1996) 161–188.
[8] B.C. Gates, H. Topsoe, Polyhedron 16 (1997) 3213–3217.
[9] D.D. Whitehurst, T. Isoda, I. Mochida, Adv. Catal. 42 (1998) 345–471.
[10] F. Bataille, J.-L. Lemberton, P. Michaud, G. Perot, M. Vrinat, M. Lemaire, E. Schulz, M. Breysse, S. Kasztelan, J. Catal. 191 (2000) 409–422.
[11] T. Kabe, A. Ishihara, Q. Zhang, Appl. Catal. A 97 (1993) L1–L9.
[12] R. Prins, Handbook of Heterogeneous Catalysis, in: G. Ertl, H. Knozinger, F. Schuth, J. Weitkamp (Eds.), 2nd ed., Wiley-VCH, Weinheim, 2008, pp. 2695–2718.
[13] V. Meille, E. Schulz, M. Lemaire, M. Vrinat, J. Catal. 170 (1997) 29–36.
[14] Y. Sun, H. Wang, R. Prins, Catal. Today 150 (2010) 213–217.
[15] D.R. Kilanowski, H. Teeuwen, B.C. Gates, V.H.J.D. Beer, G.C.A. Schuit, H. Kwart, J.Catal 55 (1978) 129–137.
[16] Q. Zhang, W. Qian, A. Ishihara, T. Kabe, J. Jpn. Petrol. Inst. 40 (1997) 185–191.
[17] T. Kabe, K. Akamatsu, A. Ishihara, S. Otsuki, M. Godo, Q. Zhang, W. Qian, Ind. Eng. Chem. Res. 36 (1997) 5146–5152.
[18] A.B. Bjerre, E. Sorensen, Ind. Eng. Chem. Res. 31 (1992) 1577–1580.
[19] X.L. Ma, K. Sakanishi, I. Mochida, Ind. Eng. Chem. Res. 35 (1996) 2487–2494.
[20] V. Lamure-meille, E. Schulz, M. Lemaire, M. Vrinat, Appl. Catal. A 131 (1995) 143–157.
[21] M. Egorova, R. Prins, J. Catal. 225 (2004) 417–427.
[22] H. Wang, R. Prins, J. Catal. 264 (2009) 31–43.
[23] A. Niquille-Röthlisberger, R. Prins, J. Catal. 242 (2006) 207–216.
[24] I.V. Babich, J.A. Moulijn, Fuel 82 (2003) 607–631.
[25] C. Song, Catal. Today 86 (2003) 211–263.
[26] S.T. Oyama, H. Zhao, H.-J. Freund, K. Asakura, R. Wlodarczyk, M. Sierka, J. Catal 285 (2012) 1–5.
[27] M. Lewandowski, P. Da Costa, D. Benichou, C. Sayag, Appl. Catal. B 93 (2010) 241–249.
[28] A. Ishihara, F. Dumeignil, J. Lee, K. Mitsuhashi, E.W. Qian, T. Kabe, Appl. Catal. A 289 (2005) 163–173.
[29] A. Niquille-Rothlisberger, R. Prins, Catal. Today 123 (2007) 198–207.
[30] H. Guo, Y. Sun, R. Prins, Catal. Today 130 (2008) 249–253.
[31] Y. Sun, R. Prins, Angew. Chem. Int. Ed. 47 (2008) 8478–8481.
[32] T. Klimova, P.M. Vara, I.P. Lee, Catal. Today 150 (2010) 171–178.
[33] R. Navarro, B. Pawelec, J.L.G. Fierro, P.T. Vasudevan, J.F. Cambra, M.B. Guemez, P.L. Arias, Fuel Process. Technol. 61 (1999) 73–88.
[34] H. Wang, E. Iglesia, ChemCatChem 3 (2011) 1166–1175.
[35] H. Wang, E. Iglesia, J. Catal. 273 (2010) 245–256.
[36] P.T. Do, W.E. Alvarez, D.E. Resasco, J. Catal 238 (2006) 477–488.
[37] J.L. Carter, G.B. McVicker, W. Weissman, W.S. Kmak, J.H. Sinfelt, Appl. Catal. 3 (1982) 327–346.
[38] G.B. McVicker, M. Daage, M.S. Touvelle, C.W. Hudson, D.P. Klein, W.C. Baird Jr., B.R. Cook, J.G. Chen, S. Hantzer, D.E.W. Vaughan, E.S. Ellis, O.C. Feeley, J. Catal. 210 (2002) 137–148.
[39] U. Nylen, L. Sassu, S. Melis, S. Jaras, M. Boutonnet, Appl. Catal. A 299 (2006) 1–13.
[40] H. Ziaei-azad, C.-X. Yin, J. Shen, Y. Hu, D. Karpuzov, N. Semagina, J. Catal. 300 (2013) 113–124.
[41] J. Cinibulk, D. Gulkova, Y. Yoshimura, Z. Vit, Appl. Catal. A 255 (2003) 321–329.
[42] A. Wajnert, M. Wojciechowska, M. Pietrowski, W. Przystajko, Catal. Commun. 9 (2008) 1493–1496.
[43] R. Navarro, Pawelec, J.L.G. Fierro, P.T. Vasudevan, J.F. Cambra, P.L. Arias, Appl. Catal. A 137 (1996) 269–286.
[44] H. Ziaei-Azad, N. Semagina, Appl. Catal. A 482 (2014) 327–335.
[45] R.J. Madon, M. Boudart, Ind. Eng. Chem. Fundam. 21 (1982) 438–447.
[46] M. Zdrazil, Catal. Today 3 (1998) 269–365.
[47] G.B. McVicker, R.T.K. Baker, R.L. Garten, E.L. Kugler, J. Catal. 65 (1980) 207–220.
[48] I. Yuranov, L. Kiwi-Minsker, A. Renken, Appl. Catal. B 43 (2003) 217–227.
[49] J. Batista, A. Pintar, D. Mandrino, M. Jenko, V. Martin, Appl. Catal. A 206 (2001) 113–124.
[50] U. Nylen, J.F. Delgado, S. Jaras, M. Boutonnet, Appl. Catal. A 262 (2004) 189–200.
[51] X. Liu, J. Phys. Chem. C 112 (2008) 5066–5073.
[52] M. Zhang, T. Yang, R. Zhao, C. Liu, Appl. Catal. A 468 (2013) 327–333.
[53] Synthesis of Solid Catalysts, in: K.P. de Jong (Ed.), Wiley-VCH, Weinheim, 2009.
[54] I. Yuranov, L. Kiwi-Minsker, P. Buffat, A. Renken, Chem. Mater. 16 (2004) 760–761.
[55] W.Z. Li, L. Kovarik, D. Mei, J. Liu, Y. Wang, C.H.F. Peden, Nat. Commun. 2481 (2013) 1–8.
[56] V. Calemma, R. Giardino, M. Ferrari, Fuel Process. Technol. 91 (2010) 770–776.
[57] R.M. Navarro, B. Pawelec, J.M. Trejo, R. Mariscal, J.L.G. Fierro, J. Catal. 189 (2000) 184–194.
[58] J.L. Rousset, L. Stievano, F.J. Cadete Santos Aires, C. Geantet, A.J. Renouprez, M. Pellarin, J. Catal. 202 (2001) 163–168.
[59] M. Egorova, R. Prins, J. Catal. 221 (2004) 11–19.
[60] M. Egorova, R. Prins, Fuel Chem. Div. Preprints 47 (2002) 445–446.